ABraytCSPfuture

Air-Brayton Cycle Concentrated Solar Power future plants via redox oxides-based structured thermochemical heat exchangers / thermal boosters

Deliverable D2.1.

Computationally-screened shortlisted redox compositions for further research

Dissemination Level: Public

WP2 Redox oxide materials powder synthesis and application-specific evaluation

Date: 31.07.2023

https://www.abraytcspfuture.eu/

This project has received funding from the European Union's Horizon Europe research and innovation programme under grant agreement no 1010845.

Disclaimer

The work described in this document has been conducted within the ABraytCSPfuture project that is co-funded by the European Union. Views and opinions expressed herein are however those of the author(s) only and do not necessarily reflect those of the European Union or of the granting authority, European Climate, Infrastructure and Environment Executive Agency (CINEA). Neither the European Union nor the granting authority can be held responsible for them.

Grant Agreement Number: 101084569 Acronym: ABraytCSPfuture				
Full Title	**A**ir-**Brayt**on Cycle **C**oncentrated **S**olar **P**ower **future** plants via redox oxides-based structured thermochemical heat exchangers/thermal boosters			
Call Topic Identifier:	HORIZON-CL5-2021-D3-03			
Funding Scheme	HORIZON EUROPE, RIA – Research and Innovation Actions			
Project start date:	01.11.2022			
Project duration:	48 months			
Project URL	https://www.abraytcspfuture.eu/			
EU Project Officer	Charles-André Lemarie			
Project Coordinator	DLR – German Aerospace Center			
Deliverable	D2.1 - Computationally-screened shortlisted redox compositions for further research			
Date of Delivery	Contractual	31.07.2023	Actual	31.07.2023
Nature	Report			
Dissemination Level	Public			
Lead Beneficiary	DLR – German Aerospace Center			

Document History

Version	**Issue Date**	**Change History**	**Authors**	**Organisation**
1.0	28.07.2023	Document drafted	Christos Agrafiotis	DLR
1.1	31.07.2023	Updated with final partner feedback	Christos Agrafiotis	DLR
1.2	31.07.2023	Final Review	Abhishek Singh	UT

About the Project

ABraytCSPfuture sets forth an innovative, carbon-neutral way for implementing the highly efficient air-Brayton gas turbine power generation cycles into future air-operated Concentrated Solar Power (CSP) plants. Air-Brayton cycles are used in traditional power plants where, however, they involve fossil fuels combustion via pressurized air. *ABraytCSPfuture*'s carbon-neutral approach aims at achieving higher solar-to-electricity efficiencies, vital for the competitiveness of CSP and non-reachable by either PVs or molten salts and thermal oils, increasing in parallel significantly the plants' storage capability. The project will develop and demonstrate a first-of-its-kind compact, dual-bed thermochemical reactor/heat exchanger unit that will transfer heat from a non-pressurised air stream to a pressurised one, while also operating as a thermal booster, raising the temperature of the pressurized stream to the level required for Brayton cycles. Furthermore, the volumetric solar energy storage density of air-operated CSP plants will be significantly increased by rendering their current sensible-only regenerative storage systems to hybrid sensible-thermochemical storage ones within the same storage volume. Both these functionalities will be materialized by thermochemical reactor/heat exchanger units comprised of non-moving, flow-through porous ceramic structures (honeycombs or foams) based on earth-abundant, cost-efficient, non-toxic oxide materials and exploiting reversible reduction/oxidation reactions of such oxides in direct contact with air, accompanied by significant endothermic/exothermic heat effects. The proposed technology is set forth by an interdisciplinary partnership spanning the entire CSP value chain, comprised of leading research centres, universities, innovative SMEs and large enterprises, including ancillary services providers and technology end-users.

Deutsches Zentrum fuer Luft- und Raumfahrt e.V., **DLR**	DE	DLR
Centre for Research & Technology Hellas, **CERTH**	EL	CERTH CENTRE FOR RESEARCH & TECHNOLOGY HELLAS
University of Twente, **UT**	NL	UNIVERSITY OF TWENTE.
Fundación CENER, **CENER**	ES	CENER NATIONAL RENEWABLE ENERGY CENTRE ADItech
Fundación TEKNIKER, **TEKN**	ES	Tekniker
Fraunhofer Gesellschaft zur Foerderung der angewandten Forschung e.V., **FHG (IWKS)**	DE	Fraunhofer IWKS
OPRA Turbines, **OPRA**	NL	OPRA AN AIREM ENERGY COMPANY
KRAFTBLOCK GmbH, **KB**	DE	KRAFT BLOCK
LANDSON Emission Technologies A/S, **LET**	DK	landson
COBRA Instalaciones y Servicios S.A., **COBRA**	ES	cobra

Table of Contents

Disclaimer 2
About the Project 3
Executive Summary 5
Changes with respect to the DoA 5
1. Introduction 6
2. Redox oxides for thermochemical energy storage 6
2.1 Phase-change oxide materials 6
2.2 Partial reduction (non-stoichiometric) oxide materials - perovskites 8
2.3 Computational studies on TCS-targeted perovskites 11
3. Computational materials screening in ABraytCSPfuture 13
4. Conclusions 16
5. References 17

This deliverable is part of a project that has received funding from the European Union's Horizon Europe research and innovation programme under grant agreement no 1010845.

Executive Summary

The present document constitutes Deliverable D2.1 "Computationally-screened shortlisted redox compositions for further research" developed within *WP2. Redox oxide materials powder synthesis and application-specific evaluation* of the HORIZON EUROPE 2020 ABraytCSPfuture project. The document describes the computational approaches and procedures followed in order to quickly screen *a priori* hundreds of redox oxide materials with respect to their potential suitability for the specific application targeted in the project, namely Thermochemical Energy Storage (TCS), and hence, guide suitable material selection strategies in a rational way from the molecular level up. Deliverable D2.1 introduces the operational characteristics, intricacies and peculiarities of perovskite materials targeted for TCS and the current literature state-of-the-art of their relevant computational screening. Then, it describes the computational procedure followed and the screening criteria applied in the ABraytCSPfuture project and culminates to a first shortlist of such redox perovskite compositions of interest to be prepared and experimentally tested, as identified through computational and thermodynamic properties' modelling and calculation of thermodynamic parameters of interest with the aid of commercial and in-house developed codes and software packages.

Changes with respect to the DoA

No changes or Deviations from the Work plan occurred with respect to this Deliverable *D2.1 Computationally-screened shortlisted redox compositions for further research.*

1. Introduction

Deliverable 2.1 is produced within the *Redox oxide materials powder synthesis and application-specific evaluation* work package (WP2) and specifically within *Task 2.1. Computational screening and optimization of redox material compositions,* wherein partners DLR, CERTH and FHG participate. The report summarizes the activities and results relevant to high-throughput computational screening and calculation of thermodynamic parameters of interest of oxide material compositions suitable for the project goals, during the first nine months of the project. To substantiate the necessity of such computational approaches, first an introduction of the concept of thermochemical energy storage (TCS) with redox oxides is presented, focusing on the peculiarities and the potential advantages of the specific oxides of interest within the ABraytCSPfuture project, namely perovskites. Then, a brief literature overview of recent relevant computational studies is provided, followed by the approach adopted in the project and the first screening results, culminating in a first shortlist of perovskite material compositions chosen for further study.

2. Redox oxides for thermochemical energy storage

2.1 Phase-change oxide materials

High-temperature thermal energy storage (TES) for efficient thermal power cycles can even out supplies from technologies using intermittent renewable energy sources, particularly those that supply high-temperature heat such as concentrating solar power (CSP). Direct coupling of the intermittent solar energy input with TES and efficient thermal power cycles like e.g. air-Brayton, may supply baseload power demands through the night and/or peak power demands in the evenings when solar irradiation drops. Thermochemical energy storage (TCS) is a promising approach to significantly increase the plant's energy storage density, by involving materials that sustain reversible endothermic reactions. These schemes operate in a cyclic mode. Under the supply of diurnal solar heat e.g. from a solar receiver of a CSP plant, a solid chemical compound reacts endothermally to form another (energy-rich) solid and a gas. The heat supplied to power this endothermic chemical reaction on-sun, can be recovered by the reverse, exothermic reaction taking place during off-sun operation [1].

Of the various solid-gas TCS material systems proposed operating through such reversible reactions (hydroxides, carbonates), oxides are advantageous because they release and absorb O_2 that can be exchanged in direct contact with ambient air. This removes the need for large and costly gas storage and compression systems and renders oxides attractive for further development to scale-up for commercial applications. TCS of solar energy with the aid of oxide materials exploits the so-called "oxygen-transfer" characteristics of oxides of multivalent metals via redox (reduction-oxidation) chemical reaction schemes that operate between the oxidized and reduced form of a metal oxide

with multiple oxidation states. In the thermal reduction (TR) step, the higher-valence oxide state – under supply of external heat – releases a fraction of its oxygen content and transforms to the lower-valence form. Exothermic oxidation of the reduced to the oxidized form via air, establishes a cyclic process scheme exploitable for TCS of solar energy. Oxides with single multivalent cations can undergo reduction at temperature ranges relevant for CSP plant power blocks, yet changing phase, as per the stoichiometry of the reaction schemes (1)-(4) shown in Table 1 [2].

Phase change redox reaction schemes	**$\Delta W_{stoichiometric}$**	**$T_{reduction}$ /$T_{oxidation}$**	**ΔH (kJ/kg)**
$2BaO_2(s) + \Delta H \rightleftarrows 2BaO(s) + O_2(g)$ ...(1)	± 9.45%	$T_{red} \approx 885^oC \approx T_{ox}$	474*
$2\ Co_3O_4(s) + \Delta H \rightleftarrows 6CoO(s) + O_2(g)$ ...(2)	± 6.64%	$T_{red} \approx 890^oC \approx T_{ox}$	844*
$6Mn_2O_3(s) + \Delta H \rightleftarrows 4Mn_3O_4(s) + O_2(g)$ ...(3)	± 3.38%	$T_{red} \approx 950^oC$ $T_{ox} \approx 690\text{-}780^oC$	204*
$6(0.8)(Mn_2O_3)*(0.2)(Fe_2O_3)(s) + \Delta H \rightleftarrows 4(0.8)(Mn_3O_4)*(0.2)*(Fe_3O_4)(s) + O_2(g)$ ...(4)	± 3.37%	$T_{red} \approx 970^oC$ $T_{ox} \approx 920^oC$	40-50
* Values from thermodynamic calculations ([5]; "kg" means "per kg of redox oxide in its oxidized state as in LHS of reaction schemes above).			

Table 1: Phase-change metal oxide systems tested for TCS; reaction schemes, respective maximum weight changes, onset reaction temperatures, reaction enthalpies.

In such materials all the cations of the multi-valent metal are transformed from the higher to the lower oxidation state during reduction upon heating and vice versa during oxidation upon cooling, at distinct, reduction/oxidation equilibrium temperatures where "abrupt" oxygen release/uptake take place in a stoichiometric proportion accompanied by the respective weight loss/gain and endothermal/exothermal effects, which typically occur within a relatively narrow temperature range (i.e. normally spanning a few tens of degrees). Early studies looked at the BaO_2/BaO (peroxide/oxide) [3] but subsequent ones in the late 1970s [4] showed that BaO_2 required very dry clean air to avoid carbonation or hydration reactions, which eventually render the redox scheme irreversible. In 2011, General Atomics rekindled interest in TCS using reducible oxides reporting thermodynamics and kinetics of phase-change single-cation oxides [5] with a particular emphasis on those exhibiting reduction reactions in the temperature ranges relevant for CSP plant power blocks. Co_3O_4/CoO and Mn_2O_3/Mn_3O_4 were identified as promising materials; however, they exhibit distinct challenges in that Co_3O_4 is high cost and high-risk material despite its exceptional energy density and reversibility and Mn_2O_3 is relatively low cost with limited performance in terms of energy density and redox kinetics. Similar behaviour can be achieved with multi-cation compositions where one cation displaces another of a similar valence but enables changes in reduction enthalpies

or redox kinetics. An example of such a multi-cation material is $Mn_xFe_{1-x}O_3$ [6] where the reaction (4) follows a similar pattern to the one of pure Mn_2O_3 (reaction 3).

2.2 Partial reduction (non-stoichiometric) oxide materials - perovskites

An alternative approach involves using oxides that can support changes in oxygen stoichiometry without necessarily changing phases. Perovskites are one of such oxide families and are actually the main target in the ABraytCSPfuture project. They are oxides comprised of at least two metal cations, of the general formula ABO_3 with A being a larger in ionic radius cation and B a relatively smaller one as shown in the schematic in Figure 1a. Furthermore, when considering suitable compositions, special attention needs to be paid to the ionic radii of the components to ensure single phase crystals are formed in the perovskite structure. Fundamental for these considerations is the so-called tolerance factor *t* introduced by Goldschmidt in 1926 [7]. This is a purely geometric ratio of ionic radii that can be calculated in its simple form as shown in Eq. (5), is additionally affected by temperature and oxidation state and indicates the stability of a multicomponent crystal with the general formula of ABO_3. A tolerance factor of 1.00 indicates that a cubic perovskite structure is stable, whereas tolerance factors above or below 1 indicate that slightly distorted variants of the ideal cubic perovskite are more stable. For instance, tolerance factors between 0.90 and 1.00 typically lead to orthorhombic or tetragonal phases, where the octahedral coordination spheres of the B cations are slightly tilted to accommodate B species with slightly larger ionic radii than in the ideal perovskite. Despite its simplicity, *t* correctly predicts the stability of many perovskites.

$$t = \frac{r_A + r_X}{\sqrt{2}(r_{B+}r_O)} \quad \ldots(5)$$

More than one cation of the same valence may occupy the A or B sites. Whereas the most common combination is $(A)^{+2}(B)^{+4}O_3$, perovskite compounds with different combinations of charged cations in the A and B sites, for example 1 + 5, 2 + 4 and 3 + 3, have also been discovered [8]. Thus, most A cations feature group I or II elements or rare earth metals, whereas B cations are often transition metals (Figure 1b). Such multivalent transition metal cations can sustain substantial fractions of vacancies on oxide ion sites to enable stoichiometries $ABO_{3-\delta}$, even in their "fully" oxidized state (denoted as $ABO_{3-\delta ox}$). In the materials of this category the reduction product does not contain all the reducible metal cations at their lower valence state but only a smaller percentage of them. Oxygen is allowed to move through and leave the lattice through the formation of oxygen vacancies without causing phase transformations that induce crystal structure disruption. Therefore, such materials react via the scheme of reaction (6a) or, more correctly under that of (6b), where (or δ_{ox} - δ_{red}, respectively. The double notation δ_{ox} - δ_{red}, can be avoided for simplicity by noting and keeping in mind that, alternatively, the extent of partial reduction δ can be > 0 even in the oxidized state). In any case, δ depends on temperature and oxygen partial pressure and is usually much smaller than 1 (for a considerable number of materials is < 0.5 in the reduced state).

Oxygen vacancies are a kind of point lattice stoichiometric defects and their mobility on the oxide surface is of great importance for redox reactions involving gases and oxides of metals with multiple oxidation states. The increase in oxide vacancy V_O site fractions (proportional to δ) is an endothermic reduction that can serve as a vehicle for TCS [1]. It is the transition metal species that are the redox-active ones in the schemes of reaction (6), whereas the charge of alkali and alkaline metals is maintained during the redox cycle.

$$ABO_3(s) + \Delta H \rightleftarrows ABO_{3-\delta}(s) + \delta/2\ O_2(g) \quad ...(6a)$$

$$ABO_{3-\delta ox}(s) + \Delta H \rightleftarrows ABO_{3-\delta red}(s) + (\delta_{red} - \delta_{ox})/2\ O_2(g) \quad ...(6b)$$

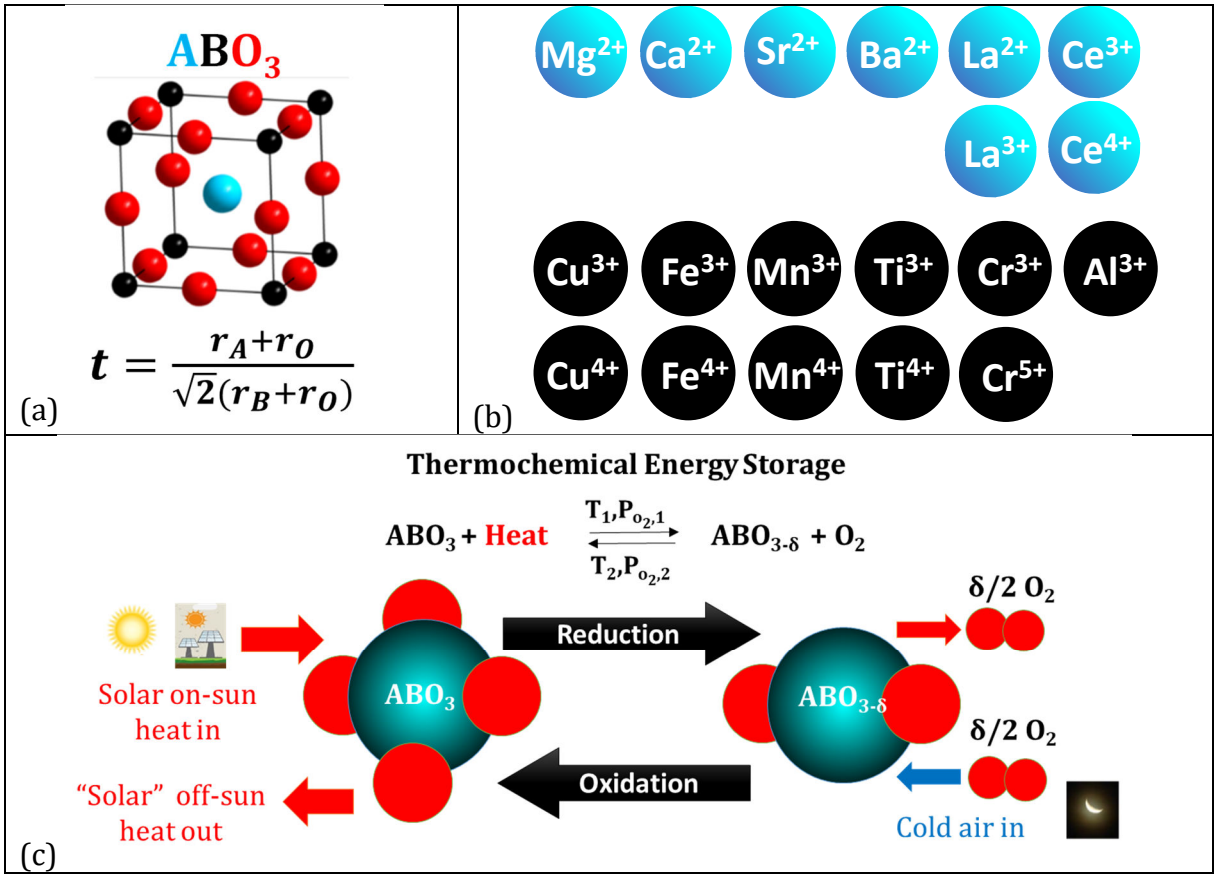

Figure 1: Schematics of (a): the perovskite unit cell, ions and tolerance factor; (b) indicative, non-exhaustive cations typically existing in perovskites; (c) thermochemical storage of solar energy implemented with perovskites-based redox cycles.

The single-phase multi-cation materials that can sustain large V_O concentrations, such as perovskites undergo reduction in a fundamentally different manner than single-cation, phase-change oxides. The equilibrium vacancy concentration $[V_O]_{eq}$ varies both with T and P_{O2} and as such reduction occurs continuously over a wide range of increasing T that can vary with P_{O2}. Likewise, re-oxidation occurs over a range of decreasing T that depends on P_{O2}. Furthermore, the presence of significant concentrations of oxide-ion vacancies in these materials supports oxide-ion conduction in the solid-phase and thus enables an additional oxygen transport mechanism within the particle [1]. Therefore, in

contrast to phase-change materials operating according to reactions (1)-(4)-, perovskites (and all materials operating via non-stoichiometric/oxygen-vacancies mechanisms) are not characterized by distinct, reduction/oxidation temperatures where "abrupt" weight loss or gain takes place; instead they release/uptake oxygen in a continuous, quasi-linear mode during the heating/cooling stages respectively within a wide temperature range that can typically span over several hundred of degrees. Consequently, the weight change corresponding to complete reaction cannot be inferred in advance from the stoichiometry of the reactants/products; instead the product's stoichiometry depends on the reduction/oxidation extent achieved at the specific experimental conditions of temperature (T) and oxygen partial pressure (P_{O2}). This implies, furthermore, that the reduction and oxidation conditions with respect to T and P_{O2}, can be different, as marked in the sketch of Figure 1c, and, hence, should be explicitly reported in every study.

$LaMnO_3$ and $CaMnO_3$ perovskites were first proposed for TCS of solar energy integrated with air-Brayton cycles in 2015 and 2016 bya team at Sandia National Laboratories [9, 10]. During the same time frame, a team from Colorado School of Mines identified alternative doped $CaMnO_3$ compositions [11, 12]. The fact that doped $CaMnO_3$ compositions – doped with Ti or Al on the A- or B-site to provide higher temperature and enthalpies of reduction [9, 10] and/or doped with Sr on the A- or B-site to provide higher reduction at lower temperatures – provides the flexibility to tune parameters with doping to tailor the performance of the perovskite for a particular TCS application. In lab-scale TGA and plugged flow reactors, these Sr-doped $CaMnO_3$ materials in particulate form sustained structural stability with high extents of reduction over 1000+ cycles [13]. A study by the French group of CNRS-PROMES on the TCS of doped barium and strontium ferrites and cobaltites (i.e., $BaCoO_3$, $BaFeO_3$, $SrCoO_3$, and $SrFeO_3$) showed that these perovskites, when reduced in very low P_{O2}, were not readily re-oxidized in air with the exception of $BaCoO_3$, which exhibited relatively high values of heat of reduction (292 kJ kg^{-1}) [14]. This stands in contrasts to the doped $CaMnO_3$-based perovskites which show rapid full re-oxidation with the use of more earth abundant cations and, up to now, are the most investigated high-temperature TCS materials.

Perovskites offer great versatility, due to the large number of cation combinations and their tunable thermodynamic characteristics, enabling additional degrees of freedom in tailoring their properties for TCS-relevant applications. With respect to the additional freedom in composition, on the one hand, material reduction temperatures can be tailored to align more closely with the heat requirements for a particular power cycle such as air-Brayton [9]. On the other hand, the ability to identify redox active compositions that rely on earth-abundant, non-critical and environmental-friendly cations provides a mechanism for driving down costs. Furthermore, the wide range of possible doping on the A or B sites in the crystalline lattice can be a significant lever by which to alter material properties such as reduction kinetics and coefficient of thermal expansion and consequently improve thermo-mechanical strength, as already demonstrated by prior work of consortium members [15-17], something very crucial in the development of structured objects.

All these features above encourage, if not necessitate, the use of atomistic-scale modelling [8] to explore compositional behaviour for preferred TCS performance before undergoing costly materials experimental testing programs. In fact, such atomistic-level simulations like Density Functional Theory (DFT) can be used to quickly screen hundreds or thousands of different compositions and guide in a rational way from the molecular level up, suitable material selection strategies. Therefore, they have become almost a necessity nowadays in order to avoid the costly, time-consuming and principally empirical or intuitive "trial-and-error" experimental synthesis and testing of a large number of compositions.

2.3 Computational studies on TCS-targeted perovskites

To support material synthesis research in a rational way, DFT calculations in combination with thermodynamic ones of the various possible reaction pairs as a function of the mixed oxides' cation valence, extent of reduction/oxidation (δ) during redox schemes and operating temperature and pressure are performed. Oxygen capacity, reaction enthalpy, and temperature and pressure operating ranges are the most critical criteria for selecting high performant TCS materials. Standard reaction enthalpy and redox oxygen capacity (expressed by δ) are critical for TCS systems since their product determines the material's TCS density. The magnitude of these properties depends naturally on the material's composition and the actual reduction procedure followed. In this respect, in the quest for materials with higher reducibility, many literature studies follow an approach based on thermodynamic modelling of the extent of reduction δ for a specific material composition as a function of temperature and oxygen partial pressure, complemented by Thermo-Gravimetric Analysis/Differential Scanning Calorimetry (TGA/DSC) experiments to determine equilibrium values, that either through the van't Hoff [18] or through point defects (oxygen vacancies) equilibrium approach [19, 20], produce P-T-δ relationships as charts of isothermal or isobaric or "iso-δ" curves. Parametric studies with respect to the kind and the quantity of the dopant elements, can then identify optimal material compositions and respective conditions for a given (or maximum possible) reduction extent, δ. In the vast majority of these thermodynamic studies, even though the temperature range spanned corresponds to that to be encountered in a solar thermal power tower plant (i.e. from 400-500°C up to 1100-1300°C), the respective pressure range usually spans very low oxygen partial pressures (from 0.21 down to 10^{-2} or 10^{-4} atm). Hence, the calculated storage densities presumably to be recovered through oxidation cited therein, usually correspond to an extent of δ achievable only under very low oxygen partial pressures. The same holds true for many "perovskite materials-screening" small-scale experimental studies aimed at quantifying these parameters, i.e. weight loss, δ and storage density as a function of operating temperature and oxygen partial pressure, usually through TGA/DSC mentioned above: reduction is performed under reduced oxygen partial pressure, equilibrium is achieved, and then re-oxidation is implemented via a stream of much higher oxygen partial pressure. However, in practical terms, the need to create very low oxygen partial pressure

environments through either vacuum or dilution with inert carrier gases, on the one hand disqualifies the inherent advantage of oxides' capability of operating in direct contact with air and on the other hand leads to low round-trip efficiencies and high costs. Therefore, it is preferable to use relatively high oxygen partial pressures from a practical standpoint. Naturally, the selection of TCS materials is also dependent upon the operating temperature range; in the specific application targeted this range has to be compatible with that of air-operating CSP plants.

DFT has shown promise in predicting the redox properties of perovskite candidates for TCS. Since, as already mentioned, oxygen defects often exist in perovskite oxides, even in their oxidized form, oxygen vacancy concentration and structure as a function of oxygen vacancy levels need to be carefully considered. A number of high-throughput computational studies on perovskites have indicated that oxygen capacity is closely related to the oxygen vacancy formation energy (Ev) and that this approach can be a useful and promising tool in guiding the screening and optimization of perovskite oxides for oxygen transfer applications [8]. As mentioned in a previous publication by DLR [21], the type of perovskite phase (cubic, or distorted) is also very important for the redox behaviour, as a DFT study [22] suggests that the cubic phase has a lower formation energy for oxygen vacancies, a finding confirmed in another publication by DLR, where doping of $CaMnO_3$ with Sr to $Ca_{0.8}Sr_{0.2}MnO_3$, decreased the distortion of the perovskite phase and consequently decreased the reduction enthalpy [19].

Targeted exactly on the development of perovskites for TCS in CSP plants, a very recent DFT study from a group in North Carolina State University employed a pressure swing between P_{O2} = 0.01 atm (reduction/energy storage) and P_{O2} = 0.2 atm (oxidation/energy release) and a temperature range between 400 and 800°C [23]. The authors selected $SrFeO_{3-\delta}$ as the parent structure, introduced various dopants to the A- and/or B-sites ($Sr_xA_{1-x}Fe_yB_{1-y}O_{3-\delta}$) and applied thermodynamic-based screening criteria to the high-throughput density functional theory (DFT) simulation results of over 2000 such A/B-site doped $SrFeO_{3-\delta}$. At a specific temperature, the Gibbs free energy (ΔG) needs to be within a suitable range to facilitate oxygen release and uptake. Given the fact that a small ΔG and a large reaction enthalpy (ΔH) are desirable for TCS, the authors used them both as the key descriptors when analyzing the results. Tolerance factors were also calculated and employed to screen out any unstable compositions. DFT calculations were performed to obtain the ΔH and ΔG of the remaining, stable compositions at different non-stoichiometry (δ) levels in the range 0.0-0.25 since experimental literature data for various TCS materials indicate that δ is usually less than 0.3 under a moderate oxygen partial pressure of >0.001 atm. In parallel, thermodynamic criteria (ΔG) for materials selection were determined based on the operational requirements. Based on the DFT prediction, 61 promising TCS candidates were selected and out of these, 45 materials with pure perovskite phases were experimentally evaluated. Many of the screened materials exhibit promising performance under practical operating conditions: $Sr_{0.875}Ba_{0.125}FeO_{3-\delta}$ exhibits a chemical energy storage density of 85 kJ/kg $ABO_{3-\delta}$ under an isobaric condition (with air) between 400 and 800 °C whereas $Sr_{0.125}Ca_{0.875}Fe_{0.25}Mn_{0.75}O_{3-\delta}$ demonstrates an energy density of 157 kJ/kg $ABO_{3-\delta}$ between 400 °C/0.2 atm O_2 and 1100 °C/0.01 atm O_2.

Another recent work employed DFT to predict the thermal characteristics of the $Ba_{1-x}Sr_xCoO_{3-\delta}$ (x = 0-1) perovskites by analyzing the electronic structures and calculated the formation energy of oxygen vacancy (Ev) that was considered as a theoretical descriptor for the reduction temperatures of the system under study [24], suggesting overall $Ba_{0.5}Sr_{0.5}CoO_{3-\delta}$ as a suitable TCS material with a reaction enthalpy of 202.20 kJ/kg.

3. Computational materials screening in ABraytCSPfuture

The starting point was a Database created by ExoMatter on behalf of DLR. This database contains 829 entries of metal oxides that are capable of a cyclic redox reaction, meaning they have at least 1 reduced and 1 oxidized state, which are stable and only differ in terms of oxygen content in the composition. Thermodynamic data, such as the formation energy, E_above_Hull (an indicator of the materials' thermodynamic stability) and the crystal structure, was collected from publicly available sources to form the database. Reaction enthalpies ΔH of the redox pairs were calculated by modelling the reduction reactions using the formation energies for each involved species. In the following, compositions are always given in their oxidized form for better clarity. It should be kept in mind that each of the 829 entries in the original database thereby represents a redox oxide pair, which contains the reduced and the oxidized state of the composition. Additional DFT calculations of solid solution compositions that were not available from other sources were performed using the Quantum Espresso package (v.6.4.1) [25, 26]. The initial crystal structures were obtained from Materials Project [27] and the Crystallography Open Database, and substituted supercells were generated using pymatgen [28]. The resulting values were processed using the ExoMatter platform. It should be noted that these calculations so far involve only the redox reaction enthalpy ΔH, which is considered independent of temperature and oxygen partial pressure in first approximation within the scope of the work described here.

In order to narrow down suitable candidates for the desired process in the project ABraytCSPFuture, an initial screening of the available database was carried out with two major impact criteria:

- the first one involved the enthalpy of the redox reaction (ΔH); in agreement with the literature results presented above in relevance to materials targeted for TCS in CSP plants, its range was set as $100 < \Delta H < 350$ kJ/mol O_2.
- the second involved the tolerance factor *t*; as elaborated above, the range was set as $0.965 < t < 1.025$ (Figure 2a) to ensure a stable perovskite structure.

These criteria narrowed down the oxide compositions to 57 entries. These are listed in Table 2, together with their calculated relevant properties of interest.

Material	Form. E. per atom	E. above hull (eV)	ΔH (kJ/mol O_2)	Tolerance factor	Space group
$Ce(SeO_4)_2$	-1.848	0	103.3	0.9868	61
$Sr_5Ca_3Fe_7CoO_{24}$	-2.172	0.03096	112.8	1.008	8
$Na_5(NiO_2)_9$	-1.154	0.0005581	114.6	0.9864	2
$Ba_2YNi_3O_8$	-2.075	0.07482	129.7	0.9696	123
$SmCrO_4$	-2.755	0	130.4	0.9877	141
$SrFeO_3$	-2.224	0	130.9	1.012	221
$Sr_3Ca(FeO_3)_4$	-2.212	0.01321	137.1	0.9939	6
$NdCrO_4$	-2.739	0	139.7	0.9989	141
$Na_3Mn_3O_8$	-1.845	0.02	142	1.022	212
$Ca_2Ni_2O_5$	-1.952	0.07543	144.7	0.9687	55
$Ca_5Cr_3O_{13}$	-2.614	0.04164	148.2	1.025	11
$Sr_6Co_4O_{13}$	-2.256	0.02873	153	0.9991	65
$Sr_{14}Fe_{14}O_{39}$	-2.278	0.01576	153.5	0.982	1
$NaFe(SeO_4)_2$	-1.424	0	155.8	1.021	12
$Sr_{10}Fe_{10}O_{29}$	-2.251	0.004819	156.3	0.982	47
$Ho_2(SeO_4)_3$	-2.089	0	168.3	0.9791	167
Na_2FeO_3	-1.638	0	172.2	0.9939	2
$Ba_3Nd_3Co_6O_{17}$	-2.267	0.0623	173.5	0.9991	12
$Ca_8Mn_6Al_2O_{21}$	-2.714	0.09064	177.9	0.9736	1
Ag_2SeO_4	-0.843	0	179.5	0.9907	70
$KBiO_3$	-1.577	0	188	0.9952	201
$Sr_{12}Fe_8O_{27}$	-2.434	0	192.9	0.982	2
$KAgO_2$	-1.029	0	193.4	0.9998	63
$EuCrO_4$	-2.503	0	201.3	0.9876	141
Na_4FeO_4	-1.634	0	201.5	0.9939	2
$Sm_2Mn_2O_7$	-2.817	0	207.6	0.9672	227
$La_2Mo_2O_9$	-2.793	0.04225	224.6	0.9807	1
$Sr_3Co_2Cl_2O_5$	-2.264	0.07507	228.9	0.9721	139
$BaNd(FeO_3)_2$	-2.398	0.06509	233.1	0.982	225
$LaNiO_3$	-2.472	0	249.3	0.9758	167
$Na_3Ni_2O_5$	-1.291	0.04112	256.3	0.9864	2
$RbAuO_2$	-1.136	0	258.8	0.9805	63
$LaCuO_3$	-2.424	0	263	1.006	167
K_3BiO_4	-1.648	0	268.7	0.9952	2
$Na_2Te_2O_7$	-1.685	0	270.9	1.007	74
$Na(CoO_2)_3$	-1.373	0	274	0.9815	12
$BaNdMnCoO_6$	-2.446	0.08627	279.4	0.9856	35
$NdCuO_3$	-2.383	0	284.4	0.9732	62
$CsTlO_2$	-1.253	0.0181	293.1	1.015	194
$Ca_2Ru_2O_7$	-2.164	0	296.3	0.986	227

Material	Form. E. per atom	E. above hull (eV)	ΔH (kJ/mol O_2)	Tolerance factor	Space group
$CaTeO_4$	-2.27	0	301.7	0.9885	60
Na_2TeO_4	-1.815	0	304.4	1.007	14
$Ba_4La_4Co_8O_{23}$	-2.297	0.05197	307.5	1.015	12
Na_2CoO_3	-1.525	0	308.6	1.022	36
$Ca_2Cu_2O_5$	-2.07	0	311.7	0.9987	33
$Ca(CuO_2)_2$	-1.71	0	314.9	0.9987	88
$Sr_4LaMn_5O_{15}$	-2.583	0.06058	316.1	0.9682	12
$Ca_8Mn_6Al_2O_{23}$	-2.678	0.06535	317.9	1.003	1
$CrPbO_4$	-1.724	0	319.6	0.9953	14
$Ba_4Sc_2Cu_2O_9$	-2.809	0	323.8	0.9957	69
$Sr_5Ca_3TiMn_7O_{24}$	-2.58	0.06764	324.7	1.003	8
$AgAsO_3$	-1.274	0	331.3	0.9694	148
$SrCa_7Mn_6Al_2O_{23}$	-2.667	0.07406	331.6	1.021	1
$NaCuO_2$	-1.355	0	332.1	1.017	63
$SrTeO_4$	-2.274	0	337.2	1.025	60
$RbTlO_2$	-1.324	0	344.3	0.9655	166
$SrCa_3Mn_4O_{12}$	-2.479	0.04892	349.9	1.022	6

Table 2: 57 redox oxide compounds with redox reaction enthalpy (ΔH): 100 < ΔH < 350 kJ/mol O_2 (column 4) and tolerance factor *t*: 0.965 < *t* < 1.025 (column 5).

A second filter was applied to exclude any non-perovskite materials from the candidate list. The calculated crystal structure was utilized as criteria for that matter. The space group is a descriptor of the crystal lattice's symmetry and an identifier of a crystal phase. All space groups not related to the perovskite structure, including the ideal cubic structure (221) as well as hexagonal (167), orthorhombic (62) and other distorted variants of lower symmetry, were removed from the list. Lastly, materials that were predicted to exhibit stable crystal phases correlated to the perovskite structure, but did not comply with the general formula ABO_3 (A and B may consist of multiple cations in stoichiometric ratios) of the perovskite material class, were manually removed from the list. This additional screening filter resulted in just 11 suitable candidate materials, which are listed in Table 3, together with their calculated properties of interest.

Material	Form. E. per atom	E. above hull (eV)	ΔH (kJ/mol O_2)	Tolerance factor	Space group
$Sr_5Ca_3Fe_7CoO_{24}$	-2.172	0.03096	112.8	1.008	8
$SrFeO_3$	-2.224	0	130.9	1.012	221
$Sr_3Ca(FeO_3)_4$	-2.212	0.01321	137.1	0.9939	6
$Ba_3Nd_3Co_6O_{17}$	-2.267	0.0623	173.5	0.9991	12
$LaNiO_3$	-2.472	0	249.3	0.9758	167
$LaCuO_3$	-2.424	0	263.0	1.006	167
$NdCuO_3$	-2.383	0	284.4	0.9732	62

Material	Form. E. per atom	E. above hull (eV)	ΔH (kJ/mol O_2)	Tolerance factor	Space group
$Ba_4La_4Co_8O_{23}$	-2.297	0.05197	307.5	1.015	12
$Sr_4LaMn_5O_{15}$	-2.583	0.06058	316.1	0.9682	12
$Sr_5Ca_3TiMn_7O_{24}$	-2.58	0.06764	324.7	1.003	8
$SrCa_3Mn_4O_{12}$	-2.479	0.04892	349.9	1.022	6

Table 3: 11 perovskite compounds with redox reaction enthalpy (ΔH): 100 < ΔH < 350 kJ/mol O_2 (column 4) and tolerance factor *t*: 0.965 < *t* < 1.025 (column 5).

Since, as already mentioned, the product of redox reaction enthalpy and redox oxygen capacity (δ) determines any material's TCS density, out of these 11 entries we can now choose three materials compositions (or small families of compositions), each one with a respective "low", "medium" and "high" redox reaction enthalpy, for further investigation:

- $SrFeO_3$ or Ca-doped $SrFeO_3$ as the "low ΔH" material with a ΔH of around 130 kJ/mol O_2
- $LaCuO_3$ or $LaNiO_3$ as the "medium ΔH" material with a ΔH of around 260 kJ/mol O_2
- Sr-doped $CaMnO_3$ (e.g. the listed 25% Sr-doped $SrCa_3Mn_4O_{12}$) as the "high ΔH" with a ΔH value of around 350 kJ/mol O_2

The next set of calculations will involve determining the thermodynamic parameters of these material families at different non-stoichiometry (δ) levels depending on the respective temperature and oxygen partial pressure "swing" applied between the two steps of the cycle. The results will be complemented by calculations of the sensible heat stored per material composition within the "temperature swing range" applied relevant to the operation of real CSP plants, to eventually lead to the final shortlisted material families exhibiting maximum overall sensible-TCS energy density that will be selected to be shaped into porous structured bodies for further testing.

4. Conclusions

A first round of computational materials screening was performed to identify a first shortlist of perovskite compositions in principle suitable for TCS of solar energy in Solar Thermal Power plants, avoiding empirical "trial-and-error" experimentation. This procedure has identified a list of three composition variations, each one with a respective "low", "medium" and "high" redox reaction enthalpy, consisting primarily (with the exception of La and Ni) of earth-abundant, low-cost, non-toxic elements. Naturally, this list is non-exhaustive and variations around these stoichiometries (e.g. slightly different dopant levels) can also be proved suitable after experimental testing. Nevertheless, it is a first rational pool of compositions to begin with, taking into consideration in parallel the current state-of-the-art and any new developments.

The screening criteria applied herein will be enriched with additional ones like e.g. Material Cost (in €/kg) and Material Carbon Footprint (in kg CO_2eq / kg) to be envisaged

as additional Columns in Tables like 2 and 3 and obtained through the interaction with Task 7.1. Life Cycle Analysis (LCA) and recyclability potential and the partners involved. The combined outcome of this screening process will culminate to the final materials selection providing relevant materials eco-friendly and cost-effective solutions roadmaps. Even though this final choice of compositions for the needs of the developmental work of the project will be made in M18, such high-throughput computational studies and further screening in Task 2.1 will continue up to M42 to provide further fundamental understanding of the mechanisms involved, ensure that there will be sufficient time for further optimization, materialize additional essential contribution in the field and form the basis for future post-project further material development.

5. References

[1] G.S. Jackson, C. Agrafiotis, S. Tescari, G. Karagiannakis, A. Ambrosini, Chapter 8: High-temperature thermochemical energy storage with oxide materials for concentrating solar applications, in: Davidson, J. (ed.), World Scientific Series on Emerging Technologies: Volume 3, Handbook of Solar Thermal Technologies Concentrating Solar Power and Fuels, Volume 2: Concentrating Solar for Thermochemical Fuels, Storage and Chemical Commodities "Concentrating Solar Thermal Power and Chemistry". World Scientific Publishing Co. Pte. Ltd (2022).

[2] C. Agrafiotis, T. Block, S. Tescari, M. Senholdt, M. Roeb, C. Sattler, Exploitation of thermochemical cycles based on solid oxide redox systems for thermochemical storage of solar heat. Part 6: testing of Mn-based combined oxides and porous structures, Solar Energy, 149, 227-244 (2017).

[3] G. Ervin, Solar heat storage using chemical reactions, Journal of Solid State Chemistry, 22, 51-61, (1977).

[4] R.G. Bowrey, J. Jutsen, Energy-storage using the reversible oxidation of barium oxide, Solar Energy. 21, 523-525, (1978).

[5] B. Wong, Thermochemical heat storage for concentrated solar power, Final Report for the U.S. Department of Energy. San Diego, CA, U.S.A. (2011).

[6] A.J. Carrillo, D.P. Serrano, P. Pizarro, J.M. Coronado, Understanding redox kinetics of iron-doped manganese oxides for high temperature thermochemical energy storage, Journal of Physical Chemistry C, 120, 27800-27812, (2016).

[7] V.M. Goldschmidt, Die Gesetze der Krystallochemie. Naturwissenschaften, 14(21), 477-485, (1926).

[8] J. Vieten, B. Bulfin, P. Huck, M. Horton, D. Guban, L. Zhu, Y. Lu, K. A. Persson, M. Roeb, C. Sattler, Materials design of perovskite solid solutions for thermochemical applications, Energy & Environmental Science, 12, 1369-1384, (2019).

[9] S.M. Babiniec, E.N. Coker, J.E. Miller, A. Ambrosini, Doped calcium manganites for advanced high-temperature thermochemical energy storage, International Journal of Energy Research, 40, 280-284, (2016).

[10] S.M. Babiniec, E.N. Coker, J.E. Miller, A. Ambrosini, Investigation of $La_xSr_{1-x}Co_yM_{1-y}O_{3-\delta}$ (M = Mn, Fe) perovskite materials as thermochemical energy storage media, Solar Energy, 118, 451-459, (2015).

[11] K.J. Albrecht, G.S. Jackson, R.J. Braun, Thermodynamically consistent modeling of redox-stable perovskite oxides for thermochemical energy conversion and storage. Applied Energy, 165, 285-296, (2016).

[12] L. Imponenti, K.J. Albrecht, R.J. Braun, G.S. Jackson, Measuring thermochemical energy storage capacity with redox cycles of doped-$CaMnO_3$, ECS Transactions, 72, 11-22, (2016).

[13] L. Imponenti, K.J. Albrecht, R. Kharait, M.D. Sanders, G.S. Jackson, Redox cycles with doped calcium manganites for thermochemical energy storage to 1000 degrees C, Applied Energy, 230, 1-18, (2018).

[14] Z.K. Zhang, L. Andre, S. Abanades, Experimental assessment of oxygen exchange capacity and thermochemical redox cycle behavior of Ba and Sr series perovskites for solar energy storage, Solar Energy, 134, 494-502, (2016).

[15] M. Pein, C. Agrafiotis, J. Vieten, D. Giasafaki, S. Brendelberger, M. Roeb, C. Sattler, Redox thermochemistry of perovskites for oxygen atmosphere control in solar-thermochemical processes, Solar Energy, 198, 612-622, (2020).

[16] M. Pein, L. Matzel, L. de Oliveira, G. Alkan, A. Francke, P. Mechnich, C. Agrafiotis, M. Roeb, C. Sattler, 'Reticulated porous perovskite structures for thermochemical solar energy storage', Advanced Energy Materials, 2102882, (2022).

[17] L. Klaas, M. Pein, P. Mechnich, A. Francke, D. Giasafaki, D. Kriechbaumer, C. Agrafiotis, M. Roeb, C. Sattler, Controlling thermal expansion and phase transitions in $Ca_{1-x}Sr_xMnO_3$ by Sr-content, Physical Chemistry Chemical Physics, 24, 27976-27988, (2022).

[18] E. Mastronardo, X. Qian, J.M. Coronado, S.M. Haile, The favourable thermodynamic properties of Fe-doped $CaMnO_3$ for thermochemical heat storage, Journal of Materials Chemistry A, 8, 8503-8517, (2020).

[19] B. Bulfin, J. Vieten, D.E. Starr, A. Azarpira, C. Zachäus, M. Hävecker, K. Skorupska, M. Schmücker, M. Roeb, C. Sattler, Redox chemistry of $CaMnO_3$ and $Ca_{0.8}Sr_{0.2}MnO_3$ oxygen storage perovskites, Journal of Materials Chemistry A, 5(17), 7912-7919, (2017).

[20] K.J. Albrecht, G.S. Jackson, R.J. Braun, Evaluating thermodynamic performance limits of thermochemical energy storage subsystems using reactive perovskite oxide particles for concentrating solar power, Solar Energy, 167, 179-193, (2018).

[21] B. Bulfin, J. Vieten, C. Agrafiotis, M. Roeb, C. Sattler, Applications and theoretical limitations of two step metal oxide redox cycles; a review, Journal of Materials Chemistry A, 5(36), 18951-18966, (2017).

[22] M. T. Curnan, J. R. Kitchin, Effects of concentration, crystal structure, magnetism, and electronic structure method on first-principles oxygen vacancy formation energy trends in perovskites, Journal of Physical Chemistry C, 118, 28776–28790, (2014).

[23] R. Cai, H. Bektas, X. Wang, K. McClintock, L. Teague, K. Yang, F. Li, Accelerated perovskite oxide development for thermochemical energy storage by a high-throughput combinatorial approach, Advanced Energy Materials, 13(18), 2203833, (2023).

[24] P. Yuan, H. Xu, Z. Ning, G. Xiao, Understanding thermochemical energy storage performance of $Ba_{1-x}Sr_xCoO_{3-\delta}$ perovskite system: A computational and experimental study, Journal of Energy Storage, 61, 106695, (2023).

[25] P. Giannozzi, S. Baroni, N. Bonini, M. Calandra, R. Car, C. Cavazzoni, D. Ceresoli, G. Chiarotti, M. Cococcioni, I. Dabo, A. Dal Corso, S. de Gironcoli, S. Fabris, G. Fratesi, R. Gebauer, U. Gerstmann, C. Gougoussis, A. Kokalj, M. Lazzeri, L. Martin-Samos, N. Marzari, F. Mauri, R. Mazzarello, S. Paolini, A. Pasquarello, L. Paulatto, C. Sbraccia, S. Scandolo, G. Sclauzero, A. Seitsonen, A. Smogunov, P. Umari, R. Wentzcovitch, QUANTUM ESPRESSO: a modular and open-source software project for quantum simulations of materials, Journal of Physics-Condensed Matter, 21 (2009).

[26] P. Giannozzi, O. Andreussi, T. Brumme, O. Bunau, M. Nardelli, M. Calandra, R. Car, C. Cavazzoni, D. Ceresoli, M. Cococcioni, N. Colonna, I. Carnimeo, A. Dal Corso, S. de Gironcoli, P. Delugas, R. DiStasio, A. Ferretti, A. Floris, G. Fratesi, G. Fugallo, R. Gebauer, U. Gerstmann, F. Giustino, T. Gorni, J. Jia, M. Kawamura, H. Ko, A. Kokalj, E. Kucukbenli, M. Lazzeri, M. Marsili, N. Marzari, F. Mauri, N. Nguyen, H. Nguyen, A. Otero-de-la-Roza, L. Paulatto, S. Ponce, D. Rocca, R. Sabatini, B. Santra, M. Schlipf, A. Seitsonen, A. Smogunov, I. Timrov, T. Thonhauser, P. Umari, N. Vast, X. Wu, S. Baroni, Advanced capabilities for materials modelling with QUANTUM ESPRESSO, Journal of Physics-Condensed Matter, 29 (2017).

[27] A. Jain, S. Ong, G. Hautier, W. Chen, W. Richards, S. Dacek, S. Cholia, D. Gunter, D. Skinner, G. Ceder, K. Persson, Commentary: The Materials Project: A materials genome approach to accelerating materials innovation, Apl Materials, 1 (2013).

[28] S. Ong, W. Richards, A. Jain, G. Hautier, M. Kocher, S. Cholia, D. Gunter, V. Chevrier, K. Persson, G. Ceder, Python Materials Genomics (pymatgen): A robust, open-source python library for materials analysis, Computational Materials Science, 68, 314-319, (2013).